MR image overlay guidance: system evaluation for preclinical use

Paweena U-Thainual, Jan Fritz, Choladawan Moonjaita, Tamas Ungi, Aaron Flammang, John A. Carrino, Gabor Fichtinger & Iulian Iordac

International Journal of Computer Assisted Radiology and Surgery
A journal for interdisciplinary research, development and applications of image guided diagnosis and therapy

ISSN 1861-6410

Int J CARS
DOI 10.1007/s11548-012-0788-0

Springer

Int J CARS
DOI 10.1007/s11548-012-0788-0

ORIGINAL ARTICLE

MR image overlay guidance: system evaluation for preclinical use

Paweena U-Thainual · Jan Fritz · Choladawan Moonjaita · Tamas Ungi · Aaron Flammang · John A. Carrino · Gabor Fichtinger · Iulian Iordachita

Received: 23 February 2012 / Accepted: 23 July 2012

Abstract
Purpose A clinical augmented reality guidance system was developed for MRI-guided musculoskeletal interventions Magnetic Resonance Image Overlay System (MR-IOS). The purpose of this study was to assess MRI compatibility, system accuracy, technical efficacy, and operator performance of the MR-IOS.
Methods and materials The impact of the MR-IOS on the MR environment was assessed by measuring image quality with signal-to-noise ratio (SNR) and signal intensity uniformity with the system in various on/off states. The system accuracy was assessed with an in-room preclinical experiment by performing 62 needle insertions on a spine phantom by an expert operator measuring entry, depth, angle, and target errors. Technical efficacy and operator performance were tested in laboratory by running an experiment with 40 novice operators (20 using freehand technique versus 20 MR-IOS-guided) with each operator inserting 10 needles into a geometric phantom. Technical efficacy was measured by comparing the success rates of needle insertions between the two operator groups. Operator performance was assessed by comparing total procedure times, total needle path distance, presumed tissue damage, and speed of individual insertions between the two operator groups.
Results The MR-IOS maximally altered SNR by 2 % with no perceptible change in image quality or uniformity. Accuracy assessment showed mean entry error of 1.6 ± 0.6 mm, depth error of 0.7 ± 0.5 mm, angle error of $1.5 \pm 1.1°$, and target error of 1.9 ± 0.8 mm. Technical efficacy showed a statistically significant difference ($p = 0.031$) between success rates (freehand 35.0 % vs. MR-IOS 80.95 %). Operator performance showed: mean total procedure time of 40.3 ± 4.4 (s) for freehand and 37.0 ± 3.7 (s) for MR-IOS ($p = 0.584$), needle path distances of 152.6 ± 15.0 mm for freehand and 116.9 ± 8.7 mm for MR-IOS ($p = 0.074$), presumed tissue damage of $7{,}417.2 \pm 955.6$ mm^2 for freehand and $6{,}062.2 \pm 678.5$ mm^2 for MR-IOS ($p = 0.347$), and speed of insertion 5.9 ± 0.4 mm/s for freehand and 4.3 ± 0.3 mm/s for MR-IOS ($p = 0.003$).
Conclusion The MR-IOS is compatible within a clinical MR imaging environment, accurate for needle placement, technically efficacious, and improves operator performance over the unassisted insertion technique. The MR-IOS was found to be suitable for further testing in a clinical setting.

Keywords Augmented reality · Percutaneous interventions · Needle guidance · Image overlay

P. U-Thainual (✉)
Department of Mechanical and Materials Engineering,
Queen's University, Kingston, ON, Canada
e-mail: paweena@jhu.edu

P. U-Thainual · G. Fichtinger · I. Iordachita
Engineering Research Center (ERC)/Laboratory for Computational Sensing and Robotics (LCSR),
Johns Hopkins University,
Baltimore, MD, USA

J. Fritz · J. A. Carrino
Russell H. Morgan Department of Radiology and Radiological Science, Johns Hopkins University School of Medicine,
Baltimore, MD, USA

C. Moonjaita
Center for Biomedical and Robotics Technology (BART LAB),
Mahidol University, Salaya,
Nakorn Pathom, Thailand

A. Flammang
Healthcare Sector, Imaging and Therapy, Siemens Corporation,
Center for Applied Medical Imaging,
Erlangen, Germany

T. Ungi · G. Fichtinger
School of Computing, Queen's University, Kingston, ON, Canada

Published online: 25 August 2012

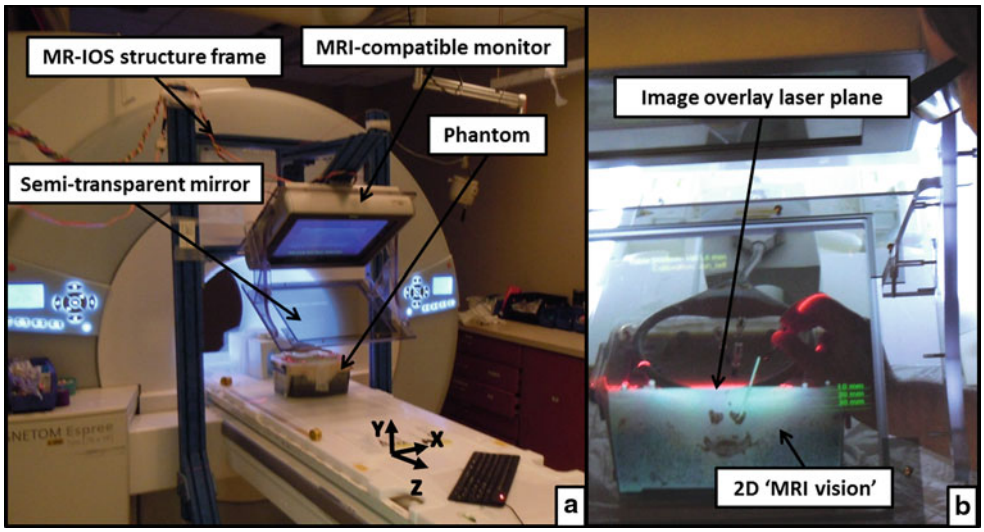

Fig. 1 **a** The MR-IOS in a phantom experiment; the system coordinates are defined as illustrated. **b** Virtual image (2D "MRI vision") superimposed on the phantom. Transverse laser plane coincides with the image projection plane

Introduction

Magnetic Resonance Imaging (MRI) is a promising interventional guidance modality, owing to its excellent tissue contrast and ability to monitor therapeutic agents, surgical tools, biomechanical tissue properties, and physiological function. Nonetheless, MRI poses formidable engineering challenges by limited access to the patient and a strong magnetic field that prevents the use of conventional materials and electronic equipment. The main challenge of image-guided needle placement procedures is how to apply the intervention plan (consisting of entry point, trajectory, and insertion depth) to the patient. Needle placement can be considered as a motion problem of 5 degrees of freedom (DOF), consisting of 3-DOF translation to the skin entry point, 2-DOF fulcrum rotation about the entry point, and 1-DOF insertion to the target along a straight trajectory. During insertion, one may apply combination of translation, rotation and oscillation to reduce resistance, tissue deformation, and needle deflection. Translation to the skin entry point can be accomplished with excellent accuracy by using skin fiducial markers. The most challenging part of the surgery is to fulcrum the needle into the correct trajectory and to maintain this direction during insertion.

In order to assist in this task, we proposed the concept of 2D MR image overlay system (MR-IOS) [1–3] (Fig. 1). In the MR-IOS, the overlay image appears to be floating inside the patient, as if the operator had tomographic vision by virtually slicing the body. This technique can also be characterized as in-situ visualization, where the medical image is rendered over the patient's body. The MR-IOS provides optically stable image from arbitrary viewpoint without auxiliary tracking instrumentation. The physician performs the intervention with the same motions as used in conventional freehand procedures. The main advantage of the MR-IOS is that the operator has optical guidance in performing the intervention without turning his/her attention away from the field of action. Previous works presented the MR-IOS concept [1–3] system design and demonstrated its basic feasibility in various clinical indications [4,5]. This paper offers detailed quantitative analysis of the MR-IOS through studies of MRI compatibility, system accuracy, technical efficacy, and operator performance.

Systems overview

Overview of the MR-IOS

The overview of the MR-IOS is in Fig. 1. We align a flat panel display and a semi-transparent mirror along their edges and mount this unit in the mouth of an imaging scanner that is able to produce 2D transverse slice images. On long bore scanners, we translate the patient out with the encoded table to position the body under the overlay. The scanner, display, and mirror are co-aligned so that the reflection of a transverse image appearing in the mirror coincides with the patient's body behind the mirror. The image seems to be suspended inside the patient in correct pose and magnification, in an optically stable position observed from any viewpoint. We acquire a transverse image, flip it horizontally, adjust its in-plane orientation and magnification, and finally render the modified image on the flat panel display. This technique can also be characterized as in-situ visualization, where the medical image is rendered right over the patient's body. Visualization and procedure planning is performed by an open-source software developed as an interactive module for 3D Slicer http://www.slicer.org.

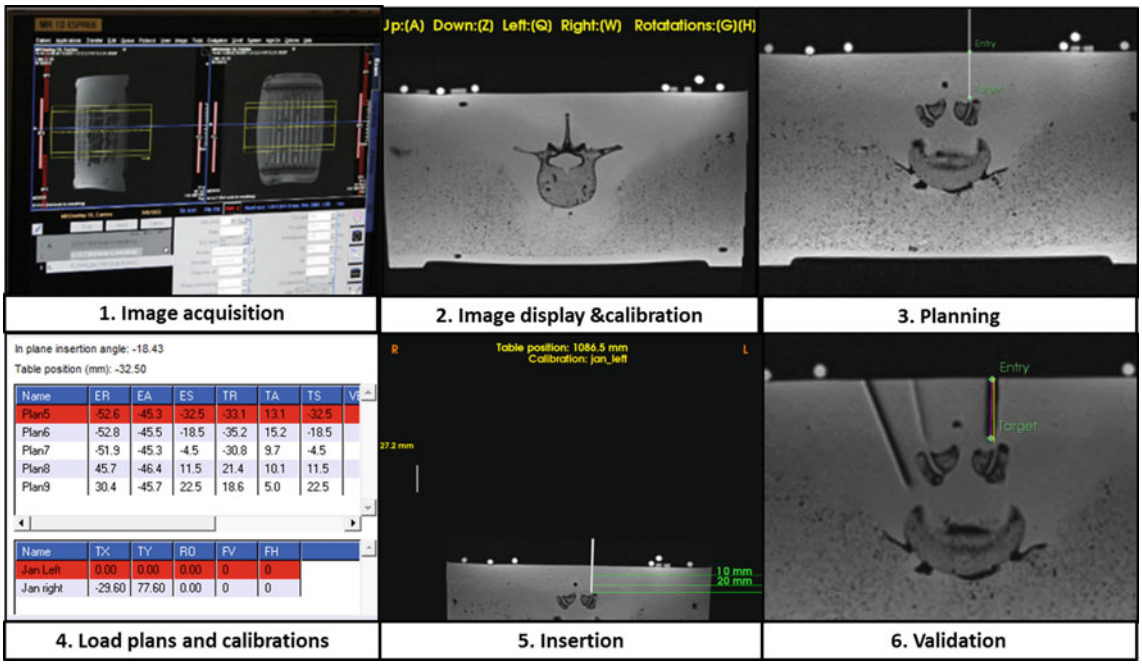

Fig. 2 MR-IOS Workflow; *1* Image acquisition, *2* Image display and calibration, *3* Planning, *4* Load plans and calibrations, *5* Insertion, and *6* Validation

A major limitation of the initial MR-IOS [1] was the inability to work adjacent to the MRI bore because of the magnetic field effects on the monitor. To overcome this disadvantage in the new system, we used a fully MRI-compatible monitor (19-inch, RF shielded LCD monitor, Siemens Healthcare) that allows the operator to work close to the bore, from 1,400 mm to less than 600 mm, minimizing table translation and allow more working space for multiple needle insertions in phantoms, cadavers, and for future clinical use.

The current MR-IOS consists of two main physically separate subsystems (in-room and out-of-room); the in-room subsystem resides in the MRI suit and consists of the main structure frame, an MRI-compatible monitor, a transverse plane laser, a semi-transparent mirror, and a wire-attached keyboard. The out-of-room subsystem resides in the MRI control room and consists of a laptop computer attached to an interconnection box (Fig. 1).

Workflow and calibration of the MR-IOS

The workflow of the MR-IOS is shown in Fig. 2. The presumed clinical workflow of the MR-IOS retains all majors of the unassisted freehand technique in musculoskeletal interventions and at any time during the procedure, the operator can revert to it. The process is as follows:

1. Image acquisition: position the subject under MR-IOS on the table and acquires a small stack of MRI images;
2. Image display and calibration: select the preferred image plane of insertion and place skin fiducials in the plane of interest. The skin fiducials are used to register the entry point picked in MRI to the actual subject;
3. Planning: the operator picks the entry and target points by mouse click. The computer marks the target and entry points, draws a virtual needle guide along the trajectory, marks the insertion depth, and provides a virtual depth gauge in the overlay image;
4. Load plans and calibrations: the subject is transferred so the image plane of interest is under the laser light of the overlay plane;
5. Insertion: the operator uses eyesight to place the needle in the middle of the laser line and virtual guided on the subject. The operator reaches behind the mirror, places the needle on the entry point, and adjusts the angle to match with the virtual guide in overlay image while holding the needle in the laser light;
6. Validation: after the needle is inserted, a confirmation image is acquired and validated.

MR-IOS calibration is based on the assumption that the virtual image plane is superimposed on the target plane. Between these two planes, there are six relative degrees of freedom that must be controlled through calibration and relative motion. Calibration of the MR-IOS is divided into three steps:

1. Hardware calibration: the virtual image plane is aligned to coincide with the overlay transverse laser plane; this is performed during the fabrication of the MR-IOS device;

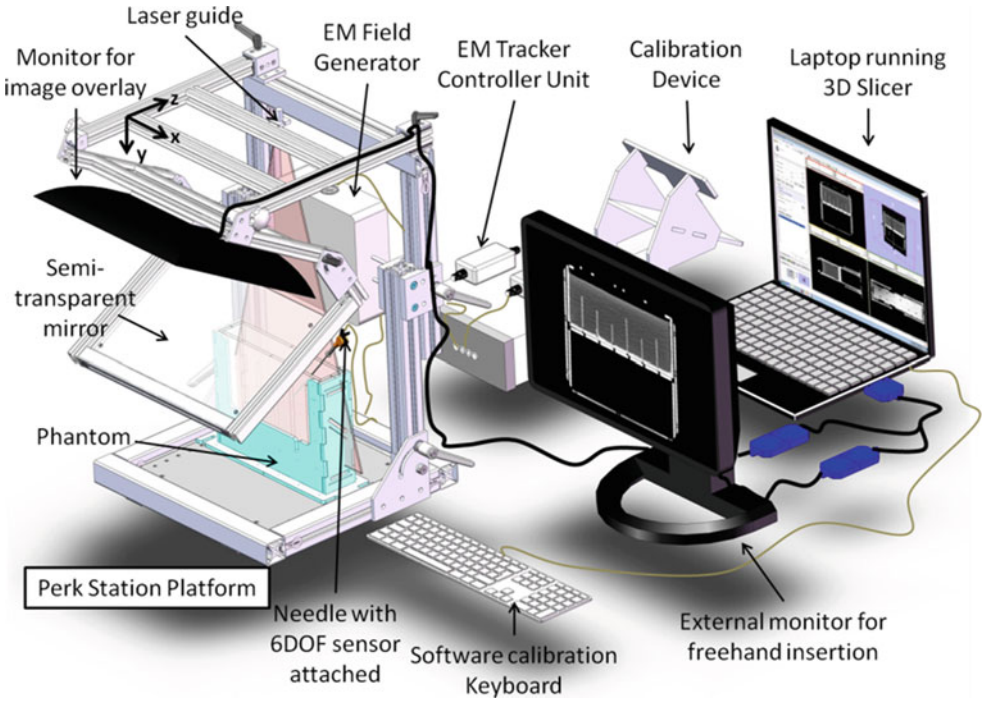

Fig. 3 Perk Station Platform for needle insertions based on 2D image overlay

2. Preprocedural system calibration: the image overlay laser plane is aligned to be parallel to the scanner laser plane; this is performed after setting the MR-IOS in front of the MRI scanner and it takes approximately 5–10 min with using a calibration phantom. During this step, the offset along the z-axis between the laser planes is measured. This step needs to be repeated before each patient. Completing Steps 1 and 2 manage three DOFs, the out of plane rotations (R_x and R_y) and translation along the z-axis (T_z);
3. Software calibration: to minimize plan offsets relative to the target (assumed to be zero), the radiologist moves the virtual image plane until the real fiducial markers on the phantom and their virtual images overlap perfectly on the phantom, by translating in the x–y directions (T_x and T_y) and rotating about the z-axis (R_z) using the keyboard; this is performed after acquiring MRI data from the phantom and it takes approximately 2 min.

The Perk Station Platform

In order to analyze operator performance of the MR-IOS over a large number of experiments and users in an economically practical manner, we detached the MR-IOS system from the scanner and translated it into a laboratory platform called Perk Station Platform (PSP), which for all practical purposes is a replica of the clinical grade MR-IOS mounted on a workbench, shown in Fig. 3 [6,7].

The operator performs needle placement in a geometric phantom containing plastic rods of 2 mm diameter as target features. An electromagnetic (EM) tracking system, NDI Aurora (Northern Digital Inc., Waterloo, ON, Canada), is used to track a phantom and needle simultaneously. The target features are registered to coordinate system of the EM tracker. A set of related coordinates are defined to enable needle tip tracking relative to the MR (or CT) images of the phantom as shown in Fig. 4. The needle tip is calibrated using the pivot calibration procedure implemented in the IGSTK software toolkit http://www.igstk.org/ and registered to the 6-DOF coil sensor (${}^{6DOF}T_{\text{tip}}$) which is recognized by the EM tracker (${}^{\text{EM}}T_{6DOF}$). The pivot points on the phantom housing are used to compute the registration transformation of the tracker to the image reference frame that load in the Slicer (${}^{\text{Slicer}}T_{\text{EM}}$) [8]. The phantom is registered to the AR overlay image slice (${}^{\text{Im}}T_{\text{Ph}}$) by relating the Z-shaped fiducials appearing on the image slice to the CAD model and to the image (${}^{\text{Slicer}}T_{\text{Im}}$), respectively. Detailed descriptions of the Perk Station, including phantom design and calibration, are available in [6,7].

System evaluation

MRI compatibility study

Running the MR-IOS may create random variations in signal intensity, which degrades image quality. To evaluate the

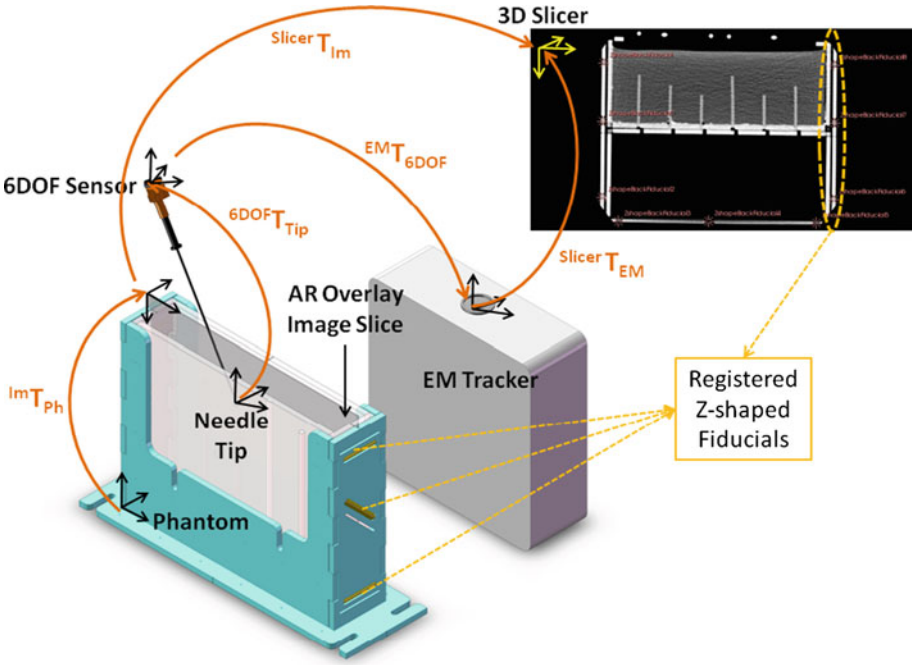

Fig. 4 Coordinate transformations in the Perk Station Platform

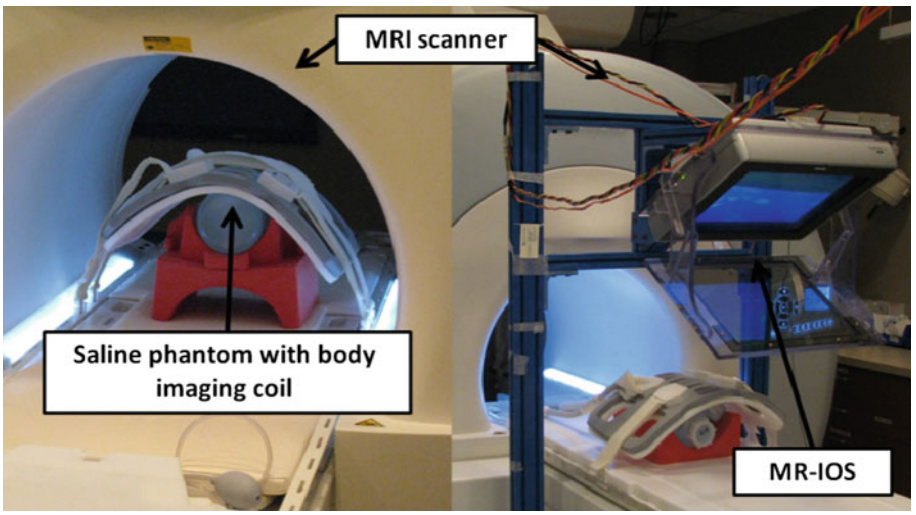

Fig. 5 MRI Compatibility study; baseline configuration *left*—acquiring five image slices of a phantom with a body imaging coil attached on top without MR-IOS being present; active configuration *right*—acquiring images with the whole system turned on

MRI compatibility of the system, we examined the signal-to-noise ratios (SNR) based on the National Electrical Manufacturers Association (NEMA) standard for determining SNR in MR images [9] while the MR-IOS was in an active and inactive state, Fig. 5. To obtain the SNR value, a set of two-dimensional axial T1-weighted fast spin echo MR images (TR/TE, 550/8.8; field-of-view, 250 × 250 mm; section thickness, 5 mm; flip angle, 90°; pixel bandwidth, 150.0) of a phantom were acquired on a 1.5-Tesla MR imaging system (Magnetom Espree, Siemens Healthcare).

The following five system configurations were used while an MR volume of five slices were acquired:

1. Baseline: images were acquired without the system in the MR room;
2. Inactive: the in-room system was setup and every component turned off;
3. Monitor only: the MR monitor was turned on;
4. Laser only: the MR monitor was turned off, and the laser was turned on;
5. Active: the complete system was turned.

Data analysis: SNR values were compared by one-way analysis of variance (ANOVA) [10].

System accuracy study

We evaluated the accuracy of the MR-IOS on a lumbar spine phantom, on a clinical MRI scanner. A total of 62 needle

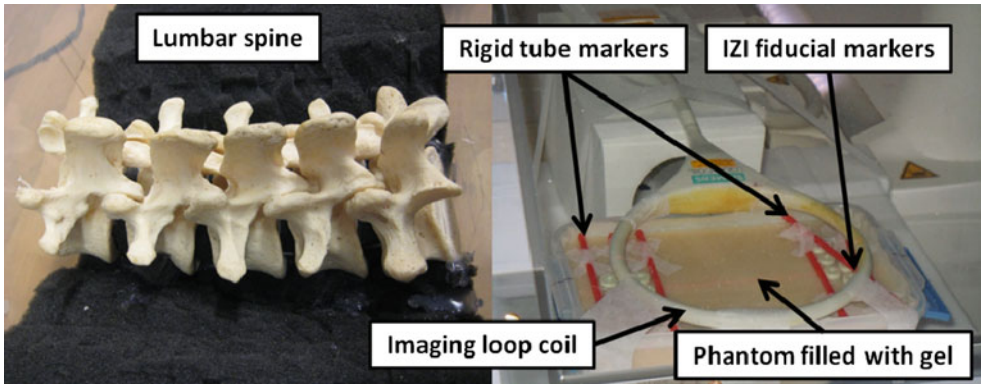

Fig. 6 Human lumbar spine phantom before filling with gel (*left*); complete phantom with fiducials markers and a receiving MRI loop coil (*right*)

insertions were employed to evaluate the technical accuracy of needle placement. MRI-compatible needles from Cook (Cook Inc., Bloomington, IN, USA) and E-Z-EM (E-Z-EM, Inc., Lake Success, NY), 20 gauge, of lengths 5, 10, and 15 cm were used according to the length of the insertion plan. The insertion depths were controlled by clippers attached to the needles. The origin of the acquired MR image was set at the iso-center of the MR scanner and was referenced by the laser planes inside the scanner bore.

Figure 6 (left) shows the human lumbar spine phantom with five lumbar vertebral bodies and foam discs, fit into a plastic enclosure with dimensions of 150 × 250 × 125 mm. The spine was embedded into an opaque soft gel (animal protein-based, SIM-TEST, Corbin Mfg. & Supply, Inc., White City, OR) simulating soft tissue and muscle as shown in Fig. 6 (right). Additionally, the top of the gel was covered with a 0.6 mm neoprene layer simulating skin. Rigid tube markers, filled with a mixture of saline (0.9 % NaCl) and gadolinium-based contrast agent in a 300:1 ratio, and a number (at least 5, depends on the region of interest) of fiducial markers (Multimodality Fiducial Marker, IZI Medical Products) were attached on the top and side of the phantom box to provide a frame of reference for the ground-truth registration of the image overlay device.

A radiologist experienced in the use of the MR-IOS performed a total of 62 needle insertions for the accuracy measurement [11]. Due to the limitation of the available targets in a spine phantom, the trials were grouped into four batches, in which the radiologist performed 14, 16, 16, and 16 insertions, respectively. The technical accuracy was assessed by the parameters of skin entry error, target error, depth error, in-plane angle error, and out-of-plane angle error. Skin entry error was defined as the Euclidean distance of the planned and actual skin entry point. The target error (mm) was defined as the Euclidean distance of the planned and actual position of the needle tips. The depth error (mm) was defined as the distance between the target locations and the needle tips along the needle trajectory. In-plane angle error (degrees) was defined as the included angle of the planned and actual needle paths. Out-of-plane angle error was defined as the deviation of the needle from the difference of needle tip between transverse image planes (entry needle tip plane and final needle tip plane). The location of the transverse image plane in 3D space was indicated using a marked line on the skin surface. Data were assessed by comparing the planned needle paths with the true locations of the needles based on pre- and postprocedure MR images 1.5-Tesla MR imaging system (Magnetom Espree, Siemens Healthcare) registered to postprocedure CT images (DynaCT, Siemens Healthcare) using the Perk Station module of 3D Slicer and were validated offline. Confirmation images were examined by the radiologist to determine the accuracy of the needle placements. Statistical analysis was performed with a statistical software package (JMP version 7.01, SAS Institute). Quantitative variables were expressed as mean ± standard deviation (SD).

The experimental setup of system accuracy assessment is shown in Fig. 7.

Technical efficacy study

The purpose of these studies was to evaluate the efficacy of the image overlay technique from the perspectives of untrained inexperienced users. We investigated the extent of external aid required given the level of skill and experience of the operator. We used the Perk Station Platform for this study. The experimental protocol for the technical efficacy study is shown in Fig. 8. Forty operators with different skill levels conducted needle placement procedures in geometrical phantoms with predefined targets. Operators were separated into two groups (freehand $N = 20$ vs. MR-IOS-guided $N = 20$). An isotropic CT data set ($n = 396$); image resolution 512 × 512; slice thickness of 0.4 mm) was acquired. Operators were provided with a tomographic image of the target and asked to insert the needle with or without guidance system based on the group. Each operator in both

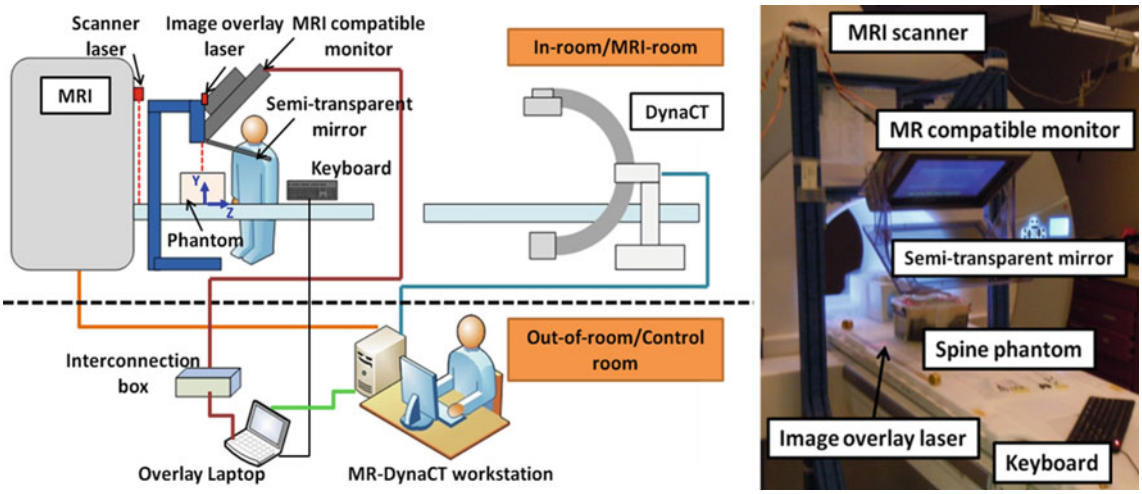

Fig. 7 System accuracy assessment; experimental setup and coordinate systems diagram (*left*) and real implementation in-room (*right*)

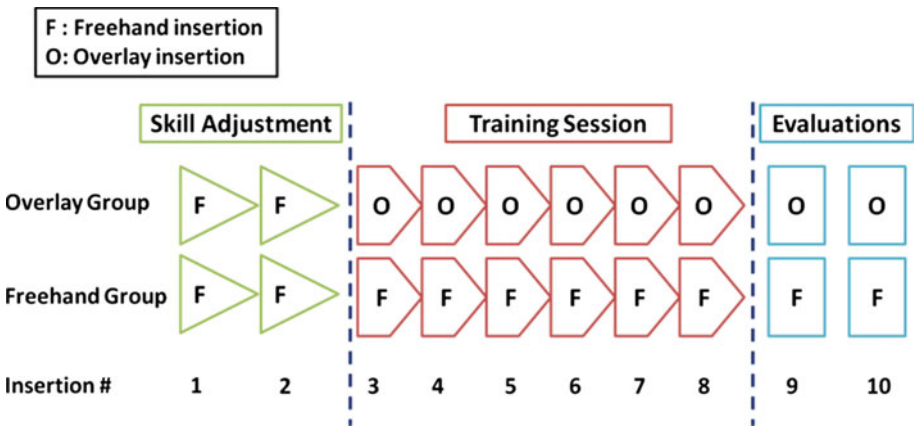

Fig. 8 Protocol of the *technical efficacy* study with a total of 10 insertions (2 skill adjustments, 6 training insertions, and 2 evaluations)

groups was asked to conduct two freehand insertions as a skill adjustment. Both groups then received a training session of six insertions, followed by two evaluation insertions. All insertions were tracked and used for analysis to compare the use of overlay versus freehand insertions. Operators were not informed of which needle insertions were training sessions and which were being assessed.

The physical layout is shown in Fig. 9. Each needle plan was initiated when the observer informs the operator that they may look at the screen, which contained the insertion plan as shown in Fig. 9 (center). The operators were required to inform the observer when they felt the needle tip in place. The observer then provided feedback to the operators regarding the success of each insertion attempt. Success was defined as physical contact of needle tip and top of the rod. Failure was defined when the needle tip did not touch the top of the rod.

Technical efficacy was measured by comparing the success rates of needle insertions between the two different image guidance techniques by using unpaired t test. Normal distribution of data was assessed with a Kolmogorov–Smirnov test. $p < 0.05$ was considered statistically significant. Quantitative variables were expressed as mean $\pm$ standard error of the mean (SEM).

Operator performance study

We conducted a study to measure operator performance using the Perk Station Platform. Needle position and orientation measurements with associated time stamps were reported by the EM tracking system. We incorporated these measurements into performance metric. Operator performance was assessed by comparing total procedure times, total needle path distance, presumed tissue damage, and speed of individual insertions. Procedure time (s) was defined as the total time spent on each insertion; starting with planning of the needle path and ending when operator indicated the final position of the needle tip. The total needle path distance (mm) was defined as the total distance of the needle tip travel inside the phantom. Presumed tissue damage (mm^2) was defined as the approximate area of tissue swept by lateral motions of the needle during the course of insertion.

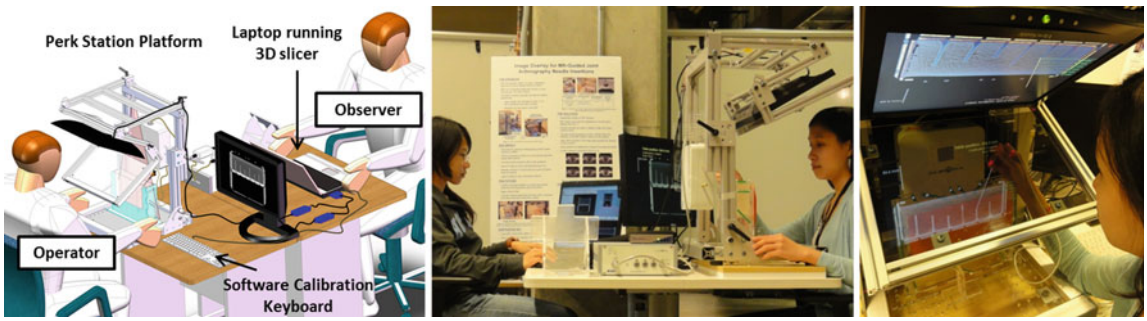

Fig. 9 Diagram of the experimental setup (*left*), the actual setup for freehand insertion (*center*), overlay insertion (*right*)

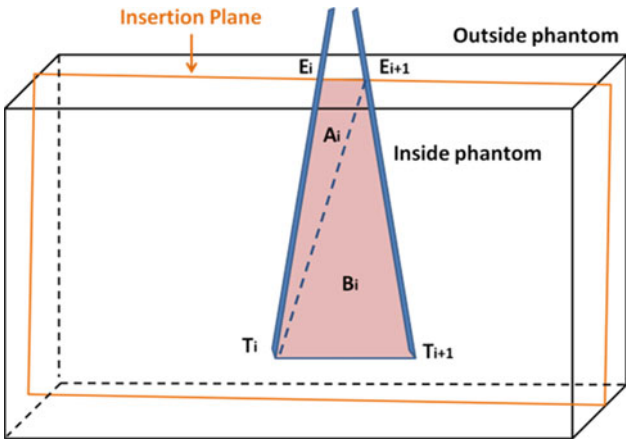

Fig. 10 Measurement of presumed tissue damage between two consecutive recorded of needle tip position, i and $i+1$. Approximate area ($A_i + B_i$) is calculated and defined by the two entry points (E) and the two tip points (T), and is not necessarily in one plane (actual insertion plane) [12]

Lateral motions were caused by attempts by the operator to adjust the needle path during insertion (We can even differentiate between in-plane and out-of-plane lateral motions, as the transverse image plane in the EM tracking coordinate system was determined during calibration). The metric was proportional with the tissue that the needle would cut due to sideways motion, illustrated in Fig. 10. The speed of insertion was defined as the ratio of the path to the total time inside the phantom. The results were analyzed by using a Mann–Whitney rank sum test and evaluated offline based on the recorded needle insertions data.

Results

MR compatibility study

MR environment compatibility assessment showed an overall SNR difference of 2 % on MR images obtained with the MR-IOS in the active and inactive state (Fig. 11). There was no perceptible change in image quality or uniformity ($p = 0.090$).

The five system configurations showed the SNR and changes as shown in Table 1 (expressed in value and percent deviation from baseline ±).

System accuracy study

All 62 needle insertions into the lumbar spine phantom were successfully accomplished. Table 2 shows the parameters that were assessed in the offline validation for accuracy includes errors in the entry and target points, insertion depth, out-of-plane angle, and in-plane angle of the insertions. The absolute errors were also determined.

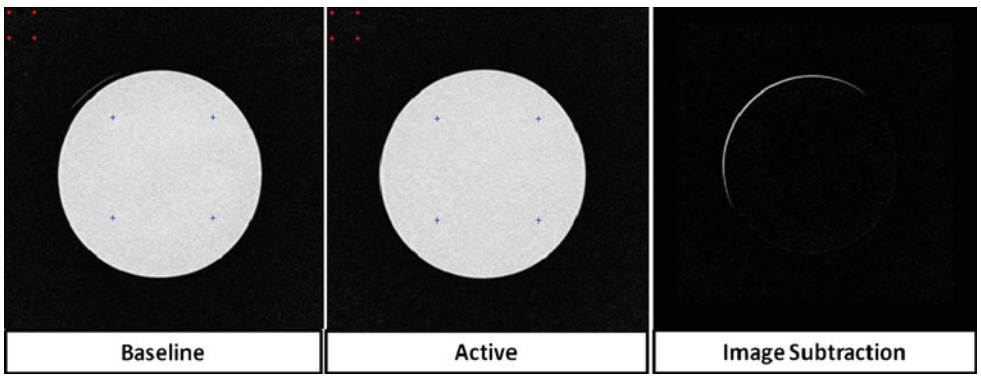

Fig. 11 Images from baseline and the system on show no visually perceptive change in uniformity as shown in image subtraction

Table 1 The SNR value and SNR (%) of each configuration

Configuration	SNR value	SNR (%)
Baseline	22	100
Inactive	23	102
Monitor only	23	101
Laser only	22	98
Active	22	98

The X–Y–Z coordinates are defined regarding to the patient; x-axis is defined along the horizontal axis from left to right; y-axis is defined along the vertical axis from anterior to posterior, and z-axis is defined along the bed from head to toe. The errors in the Z-direction are shown to be consistently increased in a single direction as shown in Fig. 12. Hence, it is attributing to the error in the target points. The data are distributed randomly in the x- and y-axes for the target points, indicating no obvious systematic errors associated with the device.

Any discrepancy could be associated with the operator. Figure 13a–c shows a plot of the plan of insertion depth (mm), in-plane angle (°), and out-of-plane angle error (°) versus absolute target error (mm); the correlation between the pairs of variables is measured by Pearson correlation. There is no significant correlation between the two. The two variables tend to be randomly spread. Figure 13d shows a plot of absolute error (mm) versus number of insertion attempt#. There is significant correlation between the two (entry and target errors) as both tend to increase together.

Technical efficacy study

Each participant performed 10 needle insertions into geometric phantom successfully. Success rate of each insertion was compared and plotted in Fig. 14. The technical efficacy of the MR-IOS was confirmed by average success rates of 80.95 % as compared to freehand insertion success rates of 35 % with a statistically significant difference ($p = 0.031$).

Operator performance study

Operator performance results are summarized in Table 3.

Data of each insertion were plotted and compared in Fig. 15a-d for total procedure time, total needle path inside phantom, presumed tissue damage, and speed of insertion, respectively. There was no statistically significant different results in the total procedure time ($p = 0.584$) and in presumed tissue damage between two groups ($p = 0.347$).

There was a significant different results in total needle path distance ($p = 0.074$) and in the speed of insertion ($p = 0.003$) between two groups.

Insertion depth versus number of success of insertions was plotted and compared in Fig. 16. Successive of insertion was decreasing in both groups with increasing target depth.

Discussion and conclusions

This study showed that the MR-IOS can be used in conjunction with a high-field clinical MR scanner and it can allow

Table 2 The mean absolute errors for 62 needle insertions defined in each parameter

Insertions	Entry error (mm)	Target error (mm)	Depth error (mm)	Out-of-plane angle error (°)	In-plane angle error (°)
62 (total)	1.6 ± 0.6	1.9 ± 0.8	0.7 ± 0.5	1.2 ± 1.3	1.5 ± 1.1

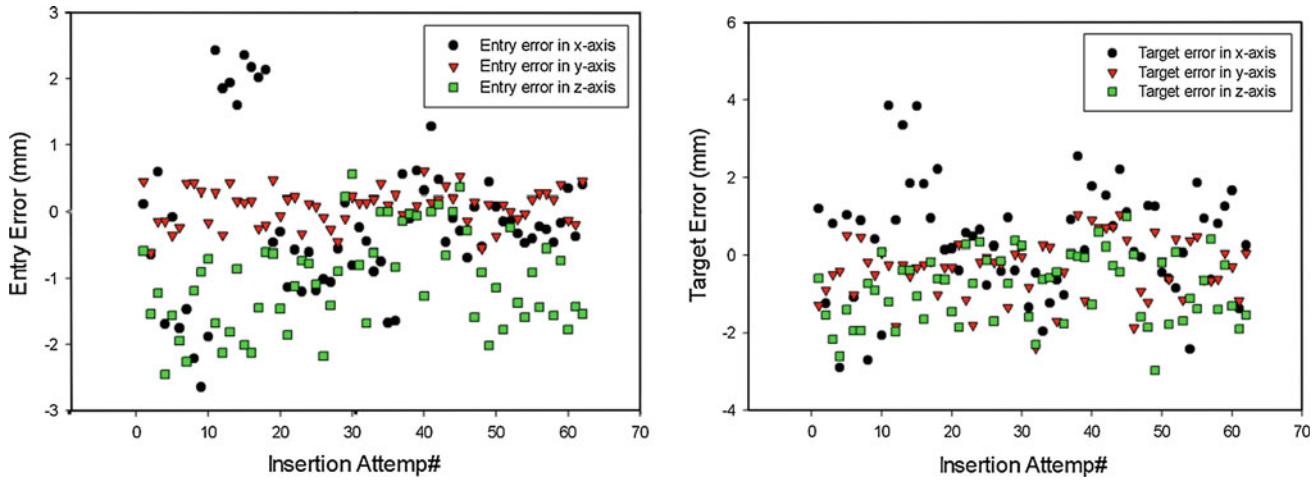

Fig. 12 Data plots of entry errors (*left*) and target errors (*right*) in $X-Y-Z$ axes

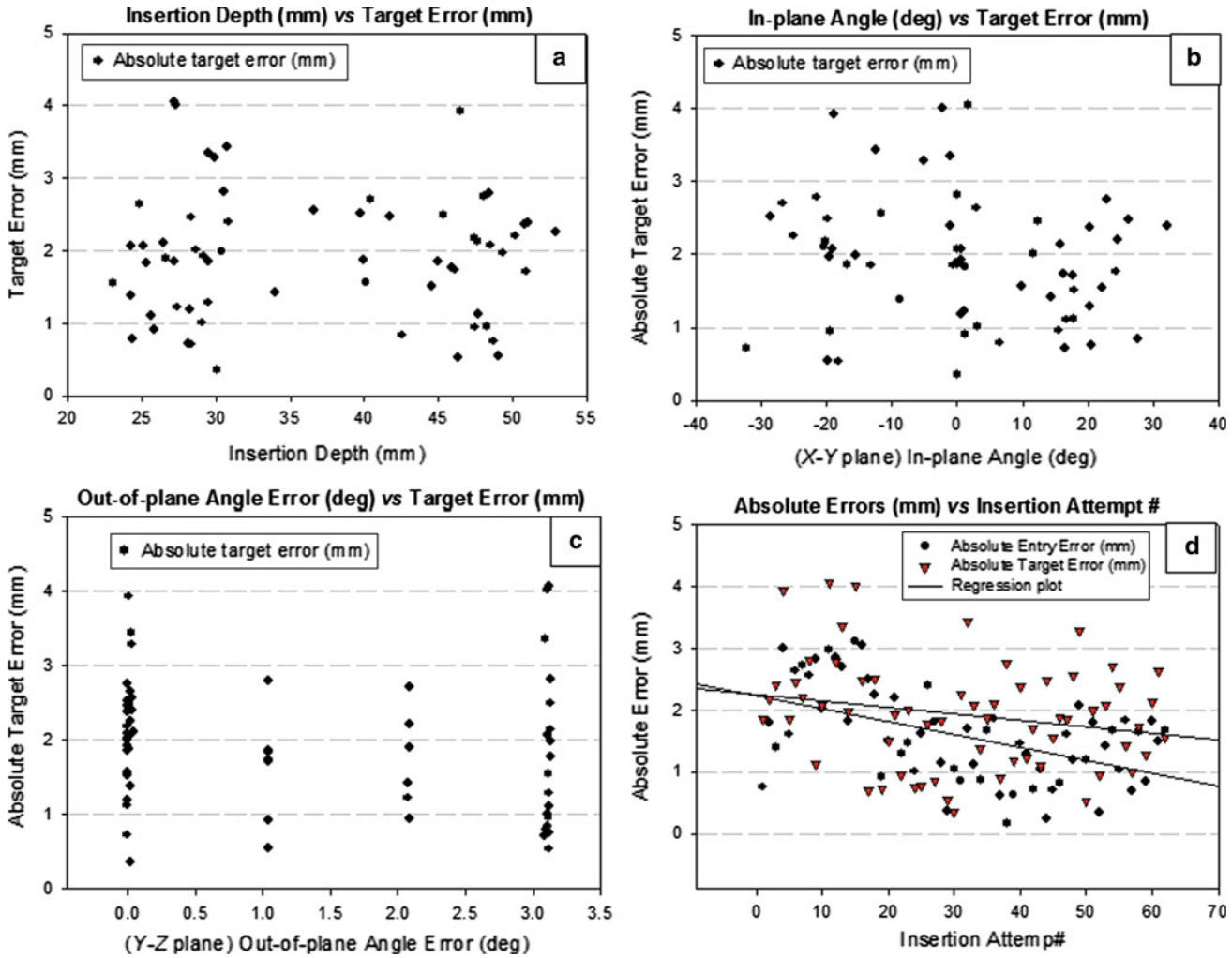

Fig. 13 Data plots of **a** insertion depth versus absolute target error; **b** in-plane angle versus absolute target error; **c** out-of plane angle error (°) versus absolute target error; and **d** insertion attempt# versus absolute error

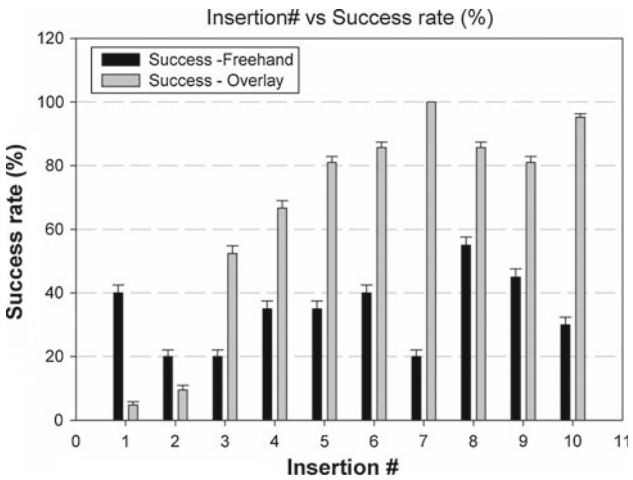

Fig. 14 Histogram of the success rate of freehand group to the overlay group by insertion attempt

for clinically accurate needle placement. Needle insertions performed using the MR-IOS have several key advantages compared to the conventional unassisted method. The distinctive advantage of the MR-IOS is that the operators use optical guidance in performing the needle placement without turning their attention away from the field of action. Moreover, accurate needle placements can be achieved with a single planning MRI scan, reducing the need for multiple in- and out-of-bore translations. The MR-IOS can be used for targeting areas that are deep and difficult to reach [1,2,13], such as epidural space injections on a lumbar spine. Lastly, there is little departure from the conventional procedure, which reduces the learning curve in using the MR-IOS technique.

This study also showed that the MR-IOS is compatible with high-field MRI scanners and it works safely and accurately right in front of the scanner's bore with only 2 % reduction in signal-to-noise ratio. As the MR-IOS does not contain

Table 3 Parameters of the evaluation of needle insertions in both groups

Parameter insertion #	Freehand	MR-IOS
Sample size	20	20
Total procedure time (s), ($p = 0.584$)	40.3 ± 4.4	37.0 ± 3.7
Total needle path distance (mm), ($p = 0.074$)	152.6 ± 15.0	116.9 ± 8.7
Presumed tissue damage (mm^2), ($p = 0.391$)	$7{,}417.2 \pm 955.6$	$6{,}062.2 \pm 678.5$
Speed of insertion (mm/s), ($p = 0.009$)	5.9 ± 0.4	4.3 ± 0.3
Success rate (%), ($p = 0.031$)	35	80.95

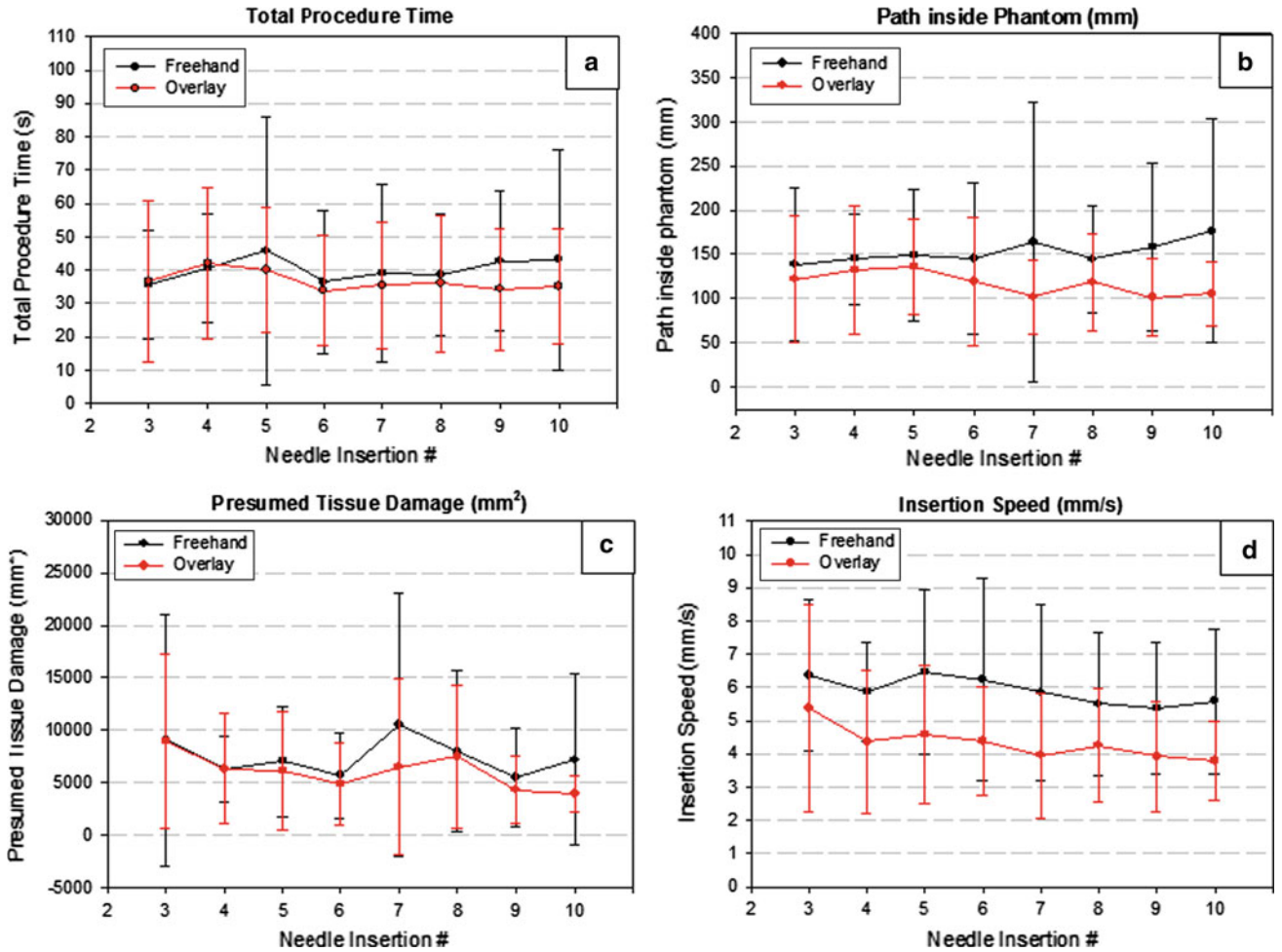

Fig. 15 Data plots of total time (s), path inside phantom (mm), possible tissue damage (mm^2), and insertion speed (mm/s) versus needle insertion #

ferromagnetic elements and does not come into contact with the patient, it is inherently MR safe according to FDA designation [14].

Needle insertion performed outside the scanner using the MR-IOS overcomes several limitations of in-bore MR imaging guidance. Space limitations inside the bore of widely available closed high-field MR imaging systems prevent MR-guided device placement inside the bore. More recently introduced MRI scanners with wide-bore design provide better patient access inside the bore; however, the distance to the iso-center interferes with accurate needle placement and sterile considerations to various degrees, depending on the procedure to be carried out. In addition, performing needle placement inside the bore generally results in the visual separation of the MR image containing the needle path and the target inside the patient, which also interferes with the

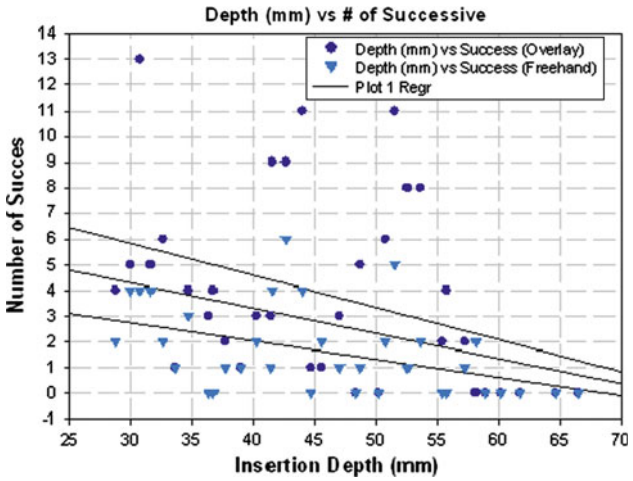

Fig. 16 Data plots of success of insertions versus depth of insertion. A sample set of trajectory plots of 4th insertion and 10th insertion from each group were plotted and compared in Figs. 17 and 18, respectively

insertion accuracy. In contrast, the MR-IOS co-locates MR image, needle path, and the target inside the patient. The view provided is similar to the one of a surgeon, supporting hand-eye coordination and improves device placement by creation of a look and feel ambiance. Because the needle placement can be carried out outside the bore, image overlay technology enables MR-guided procedures with closed MRI scanners that were previously not possible, generally improves patient access, workflow and device action, and lastly possibly improve accuracy.

The proposed calibration methodology employs cross-sectional imaging as the reference standard and demonstrates improvement of the accuracy of better than 2 mm. By grouping the overall error into multiple components, it was possible to quantify the contribution of different sources of error. There are three potential sources of error along the long axis of the gantry and table. One source of error is related to the operator's skill and experience. The other two sources of error are related to the system. We measured the distance between the scanner's iso-center and the table's current position with a tape ruler affixed to the table, serving as a point of reference. We did not use the system's inbuilt electronic table encoder in this study. We noticed an occasional disagreement between the electronic encoder and the reading from the ruler. The source and the nature of the discrepancy were not investigated in this study. The second source of system-related error involves optical refraction in the mirror. This influences the distance between the physical location of the target and its apparent location in the image, as it is measured at the surface of the refracting medium. The refraction error causes the needle to appear shifted from its true

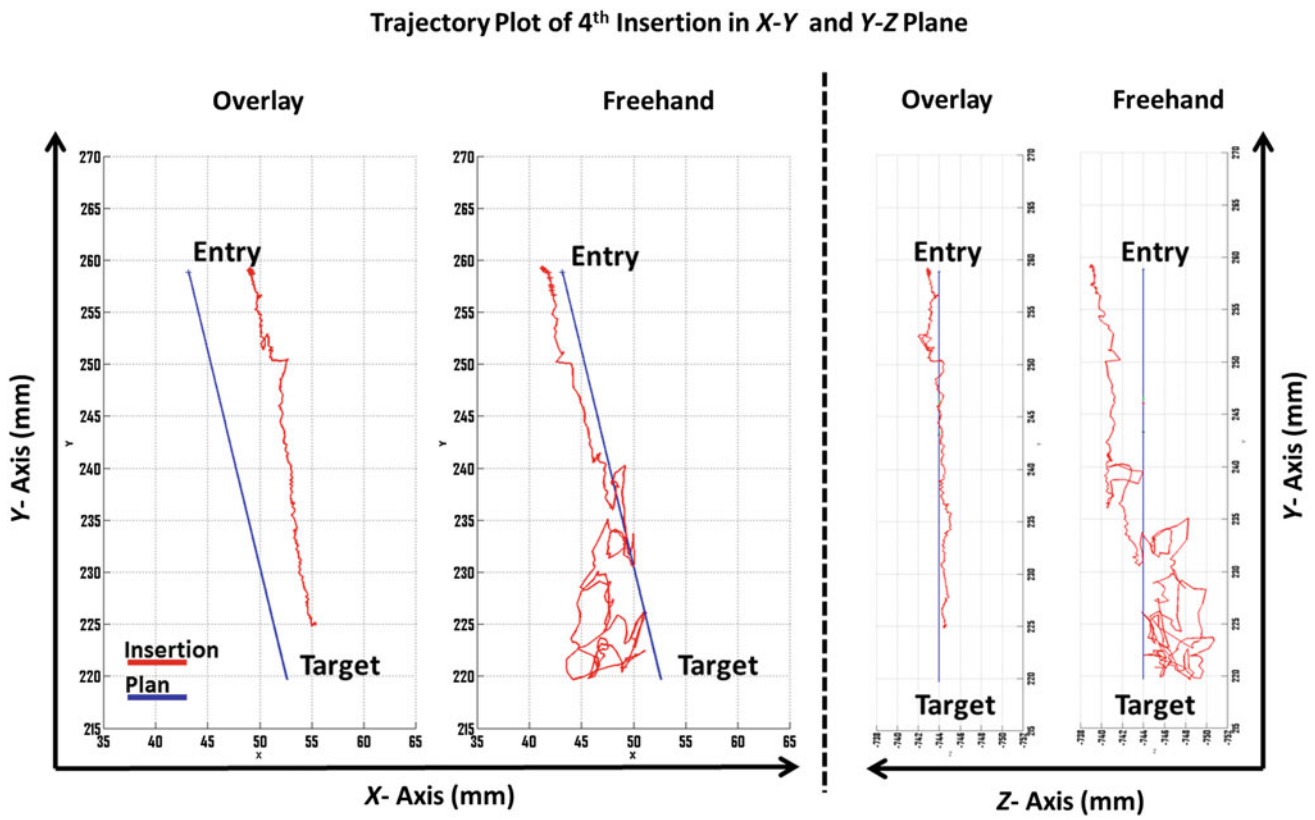

Fig. 17 Trajectories plots of 4th insertion of freehand and overlay group

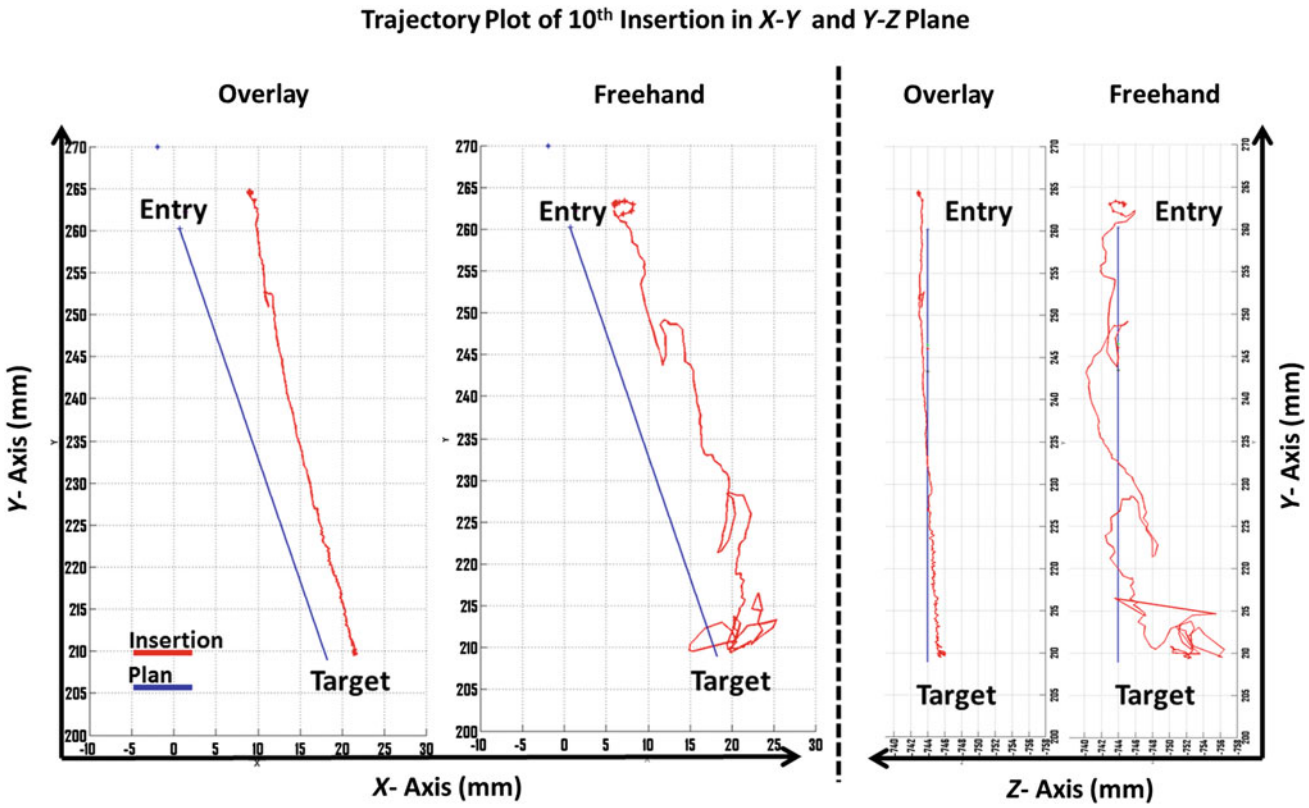

Fig. 18 Trajectory plots of 10th insertion of freehand and overlay group

position. By applying Snell's law of reflection for the mirror of 3.2 mm thickness and assuming a typical viewing angle of about 45°, we estimate the error due to refraction to be less than 2 mm.

The refraction error disappears when the operator looks into mirror perpendicularly, which fairly easy to do during surgery. The refraction error is considered only in moving the needle to the skin entry point, because afterward the needle is simply held parallel to the virtual guide.

The total procedure time does not differ significantly between the freehand and MR-IOS groups. The overlay group shows significant improvement with respect to maintaining a steady hand during insertion, indicated by a more direct and shorter needle path and less lateral needle motion causing tissue damage. There is no difference in insertion speed between the two groups. While the freehand group generally achieved a final position with greater speed, there was no guarantee of reaching the target. A possible explanation for this phenomenon is that the freehand group did not correctly position the needle at the entry point. Then, they tried to compensate for this initial error by repositioning or rotating needle inside the tissue, leading to longer travel of the needle tip and greater tissue damage. Generally, the freehand group also tended to be more uncertain with the needle direction, which they compensated by repositioning and rotating the needle, they affect the speed of insertion. The overlay group tended to insert the needle more slowly as they were simply followed the guidance path. Additionally, the overlay group never missed the skin entry point, so the need to reposition was less than in the freehand group. Overall, using overlay guidance did not increase needle insertion time.

The overlay group produced consistently higher success rates, up to 80 % in operators previously unfamiliar with percutaneous needle placement. The trajectory plots show the steadiness of the hand during insertion compared to the freehand group. The histogram showing success rate by insertion attempt (Fig. 14) suggests a positive training effect with the MR-IOS, as further insertions show a higher success rate, while this relationship is not evident for the freehand group. Using inexperienced operators in the studies provides a first approximation of potential benefit for trainees. In addition, the accuracy plot of error versus insertion attempt (Fig. 13d) also suggests a training effect even for an expert user.

In conclusion, we found that the MR-IOS was compatible with high-field MRI scanners, allowed for accurate for needle placement, it was technically efficacious and it improved operator performance over the freehand insertion technique. We conclude that the MR-IOS is suitable for further testing in a clinical setting.

Acknowledgments This project is funded by National Institutes of Health grant #R01 CA118371 A2. Paweena U-Thainual was supported by the Natural Sciences and Engineering Research Council of Canada. Gabor Fichtinger was supported as a Cancer Care Ontario Research Chair. Tamas Ungi was supported as Ontario Ministry of Research and Innovation Fellow. Choladawan Moonjaita was supported by the Center for Biomedical and Robotics Technology (BART LAB), Mahidol University, Thailand.

Conflict of interest None.

References

1. Fischer GS, Deguet A, Csoma C, Taylor RH, Fayad LM, Carrino JA, Zinreich SJ, Fichtinger G (2007) MRI image overlay: application to arthrography needle insertion. J Comput Assis Surg JCAS 12(1):2–14
2. Fischer GS, Deguet A, Csoma C, Taylor RH, Fayad L, Zinreich SJ, Fichtinger G (2006) Musculoskeletal needle placement with MRI image overlay guidance. International society for computer assisted orthopaedic surgery 6th annual conference—CAOS 2006, Montreal, pp 158–160
3. Fischer GS, Dyer E, Csoma C, Deguet A, Fichtinger G (2007) Validation system of MRI image overlay and other insertion techniques. Studies in health technology and informatics—medicine meets virtual reality. In vivo, In vitro, In silico: Designing the Next in Medicine 15(125):130–135
4. Fritz J, U-Thainual P, Ungi T, Flammang AJ, Cho NB, Fichtinger G, Iordachita I, Carrino JA (2012) Augmented reality visualization using image-overlay for MR-Guided interventions: accuracy for lumbar spinal procedures with a 1.5 Tesla MRI scanner. Am J Roentgenol 198(3):W266–W273
5. Fritz J, U-Thainual P, Ungi T, Flammang AJ, Cho NB, Fichtinger G, Iordachita I, Carrino JA (2011) Augmented reality visualization using image-overlay for MR-guided interventions: assessment of performance in cadaveric shoulder and hip arthrography. RSNA 97th Scientific Assembly and Annual Meeting
6. U-Thainual P, Fischer G, Iordachita I, Vikal S, Fichtinger G (2009) The Perk Station: systems design for percutaneous intervention training suite. In: Proceedings IEEE international conference on robotics and biomimetics ROBIO 2009, Bangkok, pp 1693–1697, 22–25 Feb, 2009
7. Vikal S, U-Thainual P, Carrino JA, Iordachita I, Fischer GS, Fichtinger G (2010) Perk Station: percutaneous surgery training and performance measurement platform. Comput Med Imaging Graph 34(1):19–32
8. Wood BJ, Zhang H, Durrani A, Glossop N, Ranjan S, Lindisch D (2005) Navigation with electromagnetic tracking for interventional radiology procedures: a feasibility study. J Vasc Interv Radiol 16(4):493–505
9. NEMA (2008) Determination of signal-to-noise ratio (SNR) in diagnostic magnetic resonance imaging, NEMA Standard Publication MS 1-2008. The association of electrical and medical imaging equipment manufacturers, 2008. http://www.nema.org/stds/ms1.cfm
10. Howell DC (2007) Statistical methods for psychology, 7th edn. Cengage Learning, Wadsworth
11. Fritz J, U-Thainual P, Ungi T, Flammang AJ, Cho N, Fichtinger G, Iordachita I, Carrino JA (2012) Augmented reality visualization with image overlay for MRI-guided intervention: accuracy for lumber spinal procedures with a 1.5-T MRI System. AJR 198:W266-W273. doi:10.2214/AJR.11.6918
12. Yeo CT, Ungi T, U-Thainual P, Lasso A, McGraw RC, Fichtinger G (2011) The effect of augmented reality training on percutaneous needle placement in spinal facet joint injections. IEEE Trans Biomed Eng 58(7):2013–2037
13. Fischer GS, Weiss CR, Dyer E, Csoma C, Deguet A, Carrino JA, Fichtinger G (2007) Evaluation of MR image overlay for spinal interventions. International society for magnetic resonance in medicine 15th scientific meeting—ISMRM 2006, Berlin, May 2007
14. http://www.fda.gov/MedicalDevices/DeviceRegulationandGuidance/GuidanceDocuments/ucm107721.htm